Fully compact higher-order computation of steady-state natural convection in a square cavity

Jiten C. Kalita,[1,*] D. C. Dalal,[1,†] and Anoop K. Dass[2,‡]
[1]*Department of Mathematics, Indian Institute of Technology, Guwahati 781039, India*
[2]*Department of Mechanical Engineering, Indian Institute of Technology, Guwahati 781039, India*
(Received 11 April 2001; published 26 November 2001)

The flow in a thermally driven square cavity with adiabatic top and bottom walls and differentially heated vertical walls for a wide range of Rayleigh numbers ($10^3 \leqslant \mathrm{Ra} \leqslant 10^7$) has been computed with a fourth-order accurate higher-order compact scheme, which was used earlier only for the stream-function vorticity (ψ-ω) form of the two-dimensional steady-state Navier-Stokes equations. The boundary conditions used are also compact and of identical accuracy. In particular, a compact fourth-order accurate Neumann boundary condition has been developed for temperature at the adiabatic walls. The treatment of the derivative source term is also compact and has been done in such a way as to give fourth-order accuracy and easy assimilation with the solution procedure. As the discretization for the ψ-ω formulation, boundary conditions, and source term treatment are all fourth-order accurate, highly accurate solutions are obtained on relatively coarser grids. Unlike other compact solution procedure in literature for this physical configuration, the present method is fully compact and fully higher-order accurate. Also, use of conjugate gradient and hybrid biconjugate gradient stabilized algorithms to solve the symmetric and nonsymmetric algebraic systems at every outer iteration, ensures good convergence behavior of the method even at higher Rayleigh numbers.

DOI: 10.1103/PhysRevE.64.066703 PACS number(s): 02.70.Bf, 47.27.Te, 47.11.+j

I. INTRODUCTION

The problem of a buoyancy driven square cavity with adiabatic top and bottom walls and differentially heated vertical walls has been the topic of extensive study in the past few decades. Along with the lid-driven cavity problem, it has become one of the most popular means for testing and validating numerical algorithms and computer codes. Some reasons for this are: (i) its simple geometry with no singularities throughout the cavity except at the corners and (ii) the availability of experimental and numerical data on this problem. The problem is also attractive because of its relevance in varied applications such as nuclear reactor insulation, ventilation of rooms, solar energy collection, crystal growth of liquids, pneumatic transport, etc. This work is concerned with the higher-order compact (HOC) computation of the problem.

The second-order (spatially) accurate schemes, particularly the central difference ones have been used in a large number of computational fluid dynamics (CFD) problems because of their straightforwardness in application. In keeping with this trend, in most of the previous attempts to tackle this problem, the schemes were at most second-order accurate in space. A time marching approach was used in the majority of the cases [1,2] to reach the steady-state solution. A second-order alternating direction implicit (ADI) scheme was used by Wilkes and Churchill [3] to produce results up to a Grashof number of 10^5; De Vahl Davis [4] presented the benchmark solutions for this problem for $\mathrm{Ra}=10^3$ to 10^6 through a second-order finite difference scheme and Richardson extrapolation; Chenoweth and Paolucci [5] used a forward time centered space (FTCS) explicit predictor corrector method; Hortman, Peric, and Scheure [6] used a finite volume multigrid method; and Ramaswamy, Jue, and Akin [7] used a second-order finite element method. The regime of high Rayleigh number was considered by Le Quéré [8] using a second-order Chebychev polynomial approach and Janssen

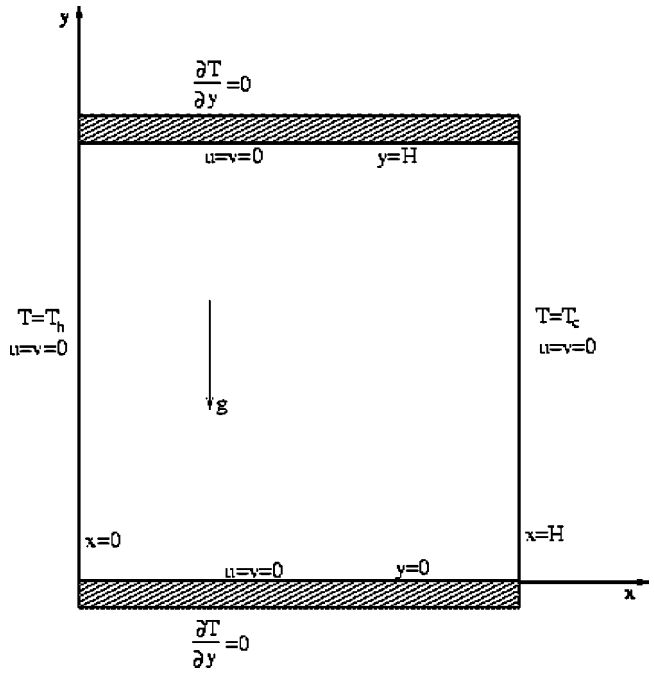

FIG. 1. A schematic view of the differentially heated square cavity.

*Author to whom correspondence should be addressed: Department of Mathematics, Indian Institute of Technology, Guwahati, North Guwahati, Assam, India. FAX: +91-361-690762. Email addresses: jiten@iitg.ernet.in and G10@postmark.net
†Email addresses: durga@iitg.ernet.in. and durga12@yahoo.com
‡Email address: anoop@iitg.ernet.in and anoop@postmark.net

TABLE I. Effect of grid size on the results for $Ra=10^3$.

Grid size	$\lvert\psi_{mid}\rvert$	u_{max} (y)	v_{max} (x)	$\overline{Nu}$	$Nu_{1/2}$	Nu_0	$Nu_{0\ max}$ (y)	$Nu_{0\ min}$ (y)	CPU time (sec)
21×21	1.178	3.647 (0.800)	3.675 (0.200)	1.116	1.120	1.115	1.494 (0.100)	0.697 (1.000)	5.66
41×41	1.176	3.642 (0.800)	3.699 (0.175)	1.117	1.118	1.117	1.503 (0.100)	0.693 (1.000)	30.75
81×81	1.175	3.650 (0.813)	3.697 (0.175)	1.118	1.118	1.118	1.505 (0.088)	0.692 (1.000)	2114.60

and Henkes [9] with a finite volume discretization with fourth-order central interpolation scheme for the convective derivatives. Recently Tagawa and Ozoe [10] carried out numerical calculations with different schemes including the Utopia and Kawamura-Kawahara scheme for low Prandtl number regime. A new pseudo-vorticity-velocity formulation and a stream function-vorticity method have been proposed by Ho and Lin [11] and Comini, Cortella, and Manzan [12], respectively. In perhaps the only previous example [13] where an HOC method was used for the problem, computations were carried out up to a Rayleigh number of 10^5. The work used $O(h^4)$ discretization of the governing equations, but the boundary treatment was not compact and the derivative source term treatment was not higher-order accurate. The present work computes the laminar solution of the problem starting with a moderate value of $Ra=10^3$ and going up to a value as high as 10^7 (with Boussinesq approximation, the flow becomes unstable at an Ra very close to 2×10^8 [5,8]) with a fourth-order accurate HOC scheme originally proposed by Spotz and Carey [14] for the ψ-ω form of the two-dimensional (2D) steady-state Navier-Stokes (N-S) equations. The temperature gradient source term in the vorticity equation is also discretized using a $O(h^4)$ compact scheme and smoothly integrated to the solution procedure. This strategy seems to have the potential of being usefully employed in similar situations, especially, to the pressure gradient term in the extension of HOC to the primitive variable formulation of the N-S equations. Also, the boundary conditions for vorticity and temperature are compact and $O(h^4)$. In particular, a compact temperature Neumann boundary condition has been developed adopting the following approach. Because of compactness and higher-order accuracy, this treatment may be taken as the model for similar computations. Thus, unlike the previous attempts, the present method is fully compact and fully higher-order accurate with associated advantages. Another attractive feature of the computation is the use of conjugate gradient (CG) [15] and hybrid biconjugate gradient stabilized (BiCGStab) [16] algorithms for solving the linear algebraic equations and this improves the convergence behavior of the algorithm. As expected, the results are very accurate and even coarse grid results compare very well with previous computations. Overall, besides opening up new possibilities, the method may be considered an efficient one for computation of flow for this physical configuration.

This paper has been arranged in five sections: Section II deals with the problem, the governing equations, and their nondimensionalizations; Sec. III with the discretization and related issues; Sec. IV with the numerical issues; and Sec. V with the results and discussion.

II. THE PROBLEM

The problem considered here is the 2D incompressible steady-state flow of a Boussinesq fluid of Prandtl number (Pr) 0.71 in an upright square cavity of side H (Fig. 1). The vertical walls are both isothermal; the left wall at temperature T_h is hotter than the right wall at temperature T_c. The horizontal walls are both insulated. Natural convection starts owing to the temperature difference between the left and right walls. Body forces are present in the form of gravitational force that acts in the negative y direction. The governing equations of the problem can be written as

$$\frac{\partial u}{\partial x}=\frac{\partial v}{\partial y}=0, \tag{1}$$

TABLE II. Effect of grid size on the results for $Ra=10^4$.

Grid size	$\lvert\psi_{mid}\rvert$	u_{max} (y)	v_{max} (x)	$\overline{Nu}$	$Nu_{1/2}$	Nu_0	$Nu_{0\ max}$ (y)	$Nu_{0\ min}$ (y)	CPU time (sec)
21×21	5.165	16.312 (0.800)	19.520 (0.150)	2.246	2.259	2.219	3.451 (0.150)	0.599 (1.000)	9.17
41×41	5.097	16.265 (0.825)	19.662 (0.125)	2.245	2.249	2.239	3.511 (0.150)	0.588 (1.000)	53.50
81×81	5.080	16.203 (0.825)	19.613 (0.125)	2.245	2.246	2.243	3.526 (0.150)	0.586 (1.000)	4051.81

TABLE III. Effect of grid size on the results for $\mathrm{Ra}=10^5$.

Grid size	$\lvert\psi_{\mathrm{mid}}\rvert$	$u_{\max}$ (y)	$v_{\max}$ (x)	$\overline{\mathrm{Nu}}$	$\mathrm{Nu}_{1/2}$	Nu_0	$\mathrm{Nu}_{0\ \max}$ (y)	$\mathrm{Nu}_{0\ \min}$ (y)	CPU time (sec)
21×21	9.172	36.375 (0.850)	66.326 (0.050)	4.507	4.502	4.321	7.001 (0.100)	0.809 (1.000)	25.49
41×41	9.142	35.156 (0.850)	68.138 (0.075)	4.522	4.523	4.479	7.519 (0.100)	0.748 (1.000)	909.45
81×81	9.123	34.825 (0.850)	68.606 (0.063)	4.522	4.522	4.512	7.670 (0.088)	0.733 (1.000)	7209.11

$$u\frac{\partial u}{\partial x}+v\frac{\partial u}{\partial y}=-\frac{1}{\rho}\frac{\partial p}{\partial x}+\nu\nabla^2 u, \tag{2}$$

$$u\frac{\partial v}{\partial x}+v\frac{\partial v}{\partial y}=-\frac{1}{\rho}\frac{\partial p}{\partial y}+g\beta(T-T_0)+\nu\nabla^2 v, \tag{3}$$

$$u\frac{\partial T}{\partial x}+v\frac{\partial T}{\partial y}=a\nabla^2 T, \tag{4}$$

where u, v, T, ρ, p, ν, a, and β are the velocity components along x and y axes, temperature, density, pressure, kinematic viscosity, thermal diffusivity, and the coefficient of thermal expansion of the fluid, respectively. T_0 is a reference temperature, g is the acceleration due to gravity and $\nabla^2 \equiv(\partial^2/\partial x^2)+(\partial^2/\partial y^2)$. The boundary conditions for the vertical walls are

$$u=v=0, \quad T=T_h \quad \text{at} \quad x=0 \quad \text{and} \quad u=v=0,$$

$$T=T_c \quad \text{at} \quad x=H\forall y, \tag{5}$$

and for the horizontal walls are

$$u=v=0. \quad \frac{\partial T}{\partial y}=0 \quad \text{at} \quad y=0 \quad \text{and} \quad y=H\forall x. \tag{6}$$

To make the above system dimensionless, we introduce the following nondimensional variables:

$$x^*=\frac{x}{H}, \quad y^*=\frac{y}{H}, \quad u^*=\frac{uH}{a}, \quad v^*=\frac{vH}{a},$$

$$T^*=\frac{T-T_0}{T_h-T_c}=\frac{T-T_0}{\Delta T}, \quad \text{and} \quad p^*=\frac{pH^2}{\rho a^2}. \tag{7}$$

The dimensionless form of the Eqs. (1)–(4) on dropping the asterisks become

$$\frac{\partial u}{\partial x}+\frac{\partial v}{\partial y}=0, \tag{8}$$

$$u\frac{\partial u}{\partial x}+v\frac{\partial u}{\partial y}=-\frac{\partial p}{\partial x}+\mathrm{Pr}\nabla^2 u, \tag{9}$$

$$u\frac{\partial v}{\partial x}+v\frac{\partial v}{\partial y}=-\frac{\partial p}{\partial y}+\mathrm{Ra}\,\mathrm{Pr}T+\mathrm{Pr}\nabla^2 v, \tag{10}$$

$$u\frac{\partial T}{\partial x}+v\frac{\partial T}{\partial y}=\nabla^2 T, \tag{11}$$

where $\mathrm{Ra}=(g\beta\Delta TH^3)/\nu a$ and $\mathrm{Pr}=\nu/a$ are the dimensionless parameters mentioned earlier. Now introducing dimensionless vorticity ω and stream-function ψ, defined by

$$\omega=\frac{\partial u}{\partial y}-\frac{\partial v}{\partial x}, \tag{12}$$

and

$$u=\frac{\partial \psi}{\partial y}, \quad v=-\frac{\partial \psi}{\partial x}, \tag{13}$$

the Eqs. (8)–(11) can be written as

$$u\frac{\partial \omega}{\partial x}+v\frac{\partial \omega}{\partial y}=\mathrm{Pr}\nabla^2\omega+\mathrm{Ra}\,\mathrm{Pr}\frac{\partial T}{\partial x}, \tag{14}$$

$$\nabla^2\psi=-\omega, \tag{15}$$

TABLE IV. Effect of grid size on the results for $\mathrm{Ra}=10^6$.

Grid size	$\lvert\psi_{\mathrm{mid}}\rvert$	$u_{\max}$ (y)	$v_{\max}$ (x)	$\overline{\mathrm{Nu}}$	$\mathrm{Nu}_{1/2}$	Nu_0	$\mathrm{Nu}_{0\ \max}$ (y)	$\mathrm{Nu}_{0\ \min}$ (y)	CPU time (sec)
21×21	15.542	63.635 (0.850)	213.397 (0.050)	8.491	8.357	7.399	11.557 (0.150)	1.267 (1.000)	575.00
41×41	16.442	66.515 (0.850)	210.696 (0.050)	8.815	8.807	8.525	15.761 (0.050)	1.095 (1.000)	2210.90
81×81	16.420	65.332 (0.850)	221.658 (0.038)	8.829	8.829	8.763	17.018 (0.050)	1.007 (1.000)	10 811.23

TABLE V. Results for Ra$=10^7$.

Grid size	$\lvert\psi_{\mathrm{mid}}\rvert$	$u_{\max}$ (y)	$v_{\max}$ (x)	$\overline{\mathrm{Nu}}$	$\mathrm{Nu}_{1/2}$	Nu_0	$\mathrm{Nu}_{0\ \max}$ (y)	$\mathrm{Nu}_{0\ \min}$ (y)	CPU time (sec)
81×81	29.382	155.82 (0.863)	696.238 (0.025)	16.517	16.513	16.075	34.925 (0.025)	1.509 (1.000)	72 843.52

$$u\frac{\partial T}{\partial x}+v\frac{\partial T}{\partial y}=\nabla^2 T. \tag{16}$$

If the reference temperature T_0 is taken as being equal to T_c, the dimensionless boundary conditions become

$$u=v=0,\quad T=1\quad \text{at}\quad x=0\quad \text{and}\quad u=v=0,$$
$$T=0\quad \text{at}\quad x=1\forall y, \tag{17}$$

and

$$u=v=0,\quad \frac{\partial T}{\partial y}=0\quad \text{at}\quad y=0\quad \text{and}\quad y=1\forall x. \tag{18}$$

The local heat flux in a horizontal direction at any point in the cavity is

$$Q(x,y)=uT-\frac{\partial T}{\partial x}. \tag{19}$$

The Nusselt number describes the heat transfer characteristics across the cavity. Through any line parallel to the y axis, the heat flow is given by

$$\mathrm{Nu}_x=\int_0^1 Q(x,y)dy. \tag{20}$$

Finally, integrating Nu_x along the horizontal direction, the average Nusselt number is computed by

$$\overline{\mathrm{Nu}}=\int_0^1 \mathrm{Nu}_x dx. \tag{21}$$

III. DISCRETIZATION AND RELATED ISSUES

A. The basic numerical scheme

The nine point variable coefficient HOC difference scheme of Spotz and Carey [14,17], originally used for the ψ-ω formulation of the 2D steady-state N-S equation, forms the core of the discretization of the present study. This HOC scheme has been obtained from the second-order central difference scheme by approximating the derivatives appearing in the second-order truncation error terms through the use of the original partial differential equation itself. Consider the steady-state 2D convection-diffusion equation for a transport variable ϕ in some domain given by

$$-\nabla^2\phi+c\frac{\partial\phi}{\partial x}+d\frac{\partial\phi}{\partial y}=f(x,y), \tag{22}$$

where c,d are the variable or constant convective coefficients and f is a forcing function. The fourth-order HOC approximation of Eq. (22) is given by [14]

$$-\alpha_{ij}\delta_x^2\phi_{ij}-\beta_{ij}\delta_y^2\phi_{ij}+C_{ij}\delta_x\phi_{ij}+D_{ij}\delta_y\phi_{ij}$$
$$-\frac{h^2}{6}[\delta_x^2\delta_y^2-c_{ij}\delta_x\delta_y^2-d_{ij}\delta_x^2\delta_y-\gamma_{ij}\delta_x\delta_y]\phi_{ij}=F_{ij}, \tag{23}$$

where δ_x and δ_y are the first and δ_x^2 and δ_y^2 are the second-order central difference operators along x and y directions, respectively, h is the uniform mesh size along both x and y directions and the coefficients α_{ij}, β_{ij}, γ_{ij}, C_{ij}, D_{ij}, and F_{ij} are as follows:

$$\alpha_{ij}=1+\frac{h^2}{12}(c_{ij}^2-2\delta_x c_{ij}), \tag{24}$$

$$\beta_{ij}=1+\frac{h^2}{12}(d_{ij}^2-2\delta_y d_{ij}), \tag{25}$$

$$\gamma_{ij}=\delta_y c_{ij}-c_{ij}d_{ij}+\delta_x d_{ij}, \tag{26}$$

$$C_{ij}=c_{ij}+\frac{h^2}{12}(\delta_x^2+\delta_y^2-c_{ij}\delta_x-d_{ij}\delta_y)c_{ij}, \tag{27}$$

$$D_{ij}=d_{ij}+\frac{h^2}{12}(\delta_x^2+\delta_y^2-c_{ij}\delta_x-d_{ij}\delta_y)d_{ij}, \tag{28}$$

$$F_{ij}=f_{ij}+\frac{h^2}{12}(\delta_x^2+\delta_y^2-c_{ij}\delta_x-d_{ij}\delta_y)f_{ij}. \tag{29}$$

Here it is assumed that the forcing function f and its derivatives are known analytically or their discrete approximations are known.

TABLE VI. Percentage errors for different Ra's.

Ra	$\lvert\psi_{\mathrm{mid}}\rvert$	$\mu_{\max}$	$\nu_{\max}$	Nu	$\mathrm{Nu}_{1/2}$	Nu_0	$\mathrm{Nu}_{0\max}$	$\mathrm{Nu}_{0\min}$
10^3	0.05	0.03	0.01	0.09	0.00	0.09	0.13	0.14
10^4	0.33	0.39	0.25	0.00	0.13	0.18	0.43	0.34
10^5	0.21	0.95	0.68	0.00	0.02	0.73	0.66	2.05
10^6	0.13	1.81	4.95	0.16	0.25	2.72	7.39	8.74

B. Discretization of the governing equations

For the vorticity equation (14), ϕ, c, d, and f in Eq. (22) are replaced by ω, u/Pr, v/Pr, and Ra$\partial T/\partial x$, respectively. The forcing function in the vorticity equation is not explicitly

TABLE VII. Comparison of $|\psi_{\mathrm{mid}}|$ for different schemes.

Ra	10^3	10^4	10^5	10^6	10^7
De Vahl Davis [4]	1.174	5.071	9.111	16.32	
Ramaswamy, Jue, and Akin [7]	1.170	5.099	9.217	16.68	29.436
Le Quéré [8]				16.38	29.362
Dennis and Hudson [13]	1.175	5.074	9.113		
Present work	1.175	5.080	9.123	16.42	29.382

known and is in derivative form. It may be mentioned that in the earlier HOC simulation of the present physical configuration [13], although the overall accuracy of the scheme was fourth, this particular source term was approximated using the standard central difference scheme at most of the points. In the following, we proceed to obtain a compact fourth-order accurate approximation of this term applying the same mechanism of using the original partial differential equation,

$$\left.\frac{\partial T}{\partial x}\right|_{ij} = \left[\delta_x T - \frac{h^2}{6}\frac{\partial^3 T}{\partial x^3}\right]_{ij} + O(h^4). \tag{30}$$

From Eq. (16),

$$\begin{aligned}\left.\frac{\partial^3 T}{\partial x^3}\right|_{ij} &= \left[-\frac{\partial^3 T}{\partial x \partial y^2} + u\frac{\partial^2 T}{\partial x^2} + \frac{\partial u}{\partial x}\frac{\partial T}{\partial x} + v\frac{\partial^2 T}{\partial x \partial y} + \frac{\partial v}{\partial x}\frac{\partial T}{\partial y}\right]_{ij},\\ &= -[\delta_x \delta_y^2 T + u\,\delta_x^2 T + \delta_x u\,\delta_x T + v\,\delta_x \delta_y T + \delta_x v\,\delta_y T]_{ij}\\ &\quad + O(h^2).\end{aligned} \tag{31}$$

Substituting Eq. (31) into Eq. (30) yields

$$\begin{aligned}\left.\frac{\partial T}{\partial x}\right|_{ij} &= \delta_x T_{ij} + \frac{h^2}{6}[\delta_x \delta_y^2 T - u\,\delta_x^2 T - \delta_x u\,\delta_x T - v\,\delta_x \delta_y T\\ &\quad - \delta_x v\,\delta_y T]_{ij} + O(h^4).\end{aligned} \tag{32}$$

Also for Eq. (15), $\phi=\psi$, $c=d=0$, and $f=\omega$. Once ω and ψ are obtained, the velocities u and v can easily be calculated in the following way:

$$u_{ij} = \left.\frac{\partial \psi}{\partial y}\right|_{ij} = \left[\delta_y \psi - \frac{h^2}{6}\frac{\partial^2 \psi}{\partial y^3}\right]_{ij} + O(h^4),$$

and using Eq. (15),

$$\begin{aligned}u_{ij} &= \delta_y \psi_{ij} - \frac{h^2}{6}\left[-\frac{\partial \omega}{\partial y} - \frac{\partial^3 \psi}{\partial x^2 \partial y}\right]_{ij} + O(h^4),\\ &= \delta_y \psi_{ij} + \frac{h^2}{6}[\delta_y \omega + \delta_x^2 \delta_y \psi]_{ij} + O(h^4).\end{aligned} \tag{33}$$

Likewise for the y component of velocity

$$v_{ij} = -\delta_x \psi_{ij} - \frac{h^4}{6}[\delta_x \omega + \delta_x \delta_y^2 \psi]_{ij} + O(h^4). \tag{34}$$

Finally, for the Eq. (16) $\phi=T$, $c=u$, $d=v$, $f=0$.

For the calculation of heat flux $Q(x,y)$ appearing in Eq. (19) across the cavity, except at $x=0$ and $x=1$, the fourth-order approximation of $\partial T/\partial x$ is computed using Eq. (31). At the vertical boundaries, to approximate $\partial T/\partial x$, along with the standard two point first-order formula, the third- and fourth-order Jensen formulas [18] have also been used. The Nusselt numbers Nu_x and $\overline{\mathrm{Nu}}$ are calculated through numerical integration using Simpson's rule.

It may be mentioned that the treatment of the first-order derivative source term mentioned earlier can easily be extended to second-order derivatives as well. One such situation arises in the solution of pressure Poisson equation at the end of a ψ-ω computation. However, the more important point is that through this source term treatment, an HOC scheme for the primitive variable form of the 2D N-S equations can be constructed as the pressure gradient term in the momentum equation and the source term in the pressure Poisson equation equation can now be handled.

TABLE VIII. Comparison of $\overline{\mathrm{Nu}}$ for different schemes.

Ra	10^3	10^4	10^5	10^6	10^7
Chenoweth and Paolucci [5]	1.118	2.244	4.520	8.822	16.82
De Vahl Davis [4]	1.118	2.243	4.519	8.800	
Le Quéré [8]				8.825	16.52
Hortmann, Peric, and Scheure [6]		2.245	4.521	8.825	
Saitoh and Hirosh [19]		2.242		8.712	
Ball and Kuo [20]	1.118	2.244	4.522	8.825	16.52
Ho and Lin [11]	1.118	2.248	4.528	8.824	16.52
Comini, Cortella, and Manzan [12]			4.503	8.825	16.53
Present work	1.118	2.245	4.522	8.829	16.52

TABLE IX. Comparison of $v_{\max}$ for different schemes.

Ra	10^3	10^4	10^5	10^6	10^7
Chenoweth and Paolucci [5]	3.695	19.62	68.63	220.8	699.0
De Vahl Davis [4]	3.697	19.62	68.63	219.4	
Ramaswamy, Jue, and Akin [7]		19.62	68.64	232.97	717.04
Le Quéré [8]				220.56	699.2
Saitoh and Hirosh [19]		19.62		216.76	
Ho and Lin [11]	3.697	19.63	68.63	219.86	705.3
Hortmann, Peric, and Scheure [6]		19.63	68.64	220.46	
Dennis and Hudson [13]	3.698	19.63	68.64		
Present work	3.697	19.61	68.61	221.66	696.2

C. HOC wall boundary conditions

The stream function ψ equals zero on the boundaries. At the corners, both u and v do not vary in the x and y directions and, therefore, the vorticity is equal to zero. Using forward differencing on the left wall [Eq. (13)],

$$v_{1,j} = -\left.\frac{\partial\psi}{\partial x}\right|_{1,j},$$
$$= -\left[\delta_x^+\psi - \frac{h}{2}\frac{\partial^2\psi}{\partial x^2} - \frac{h^2}{6}\frac{\partial^3\psi}{\partial x^3} - \frac{h^3}{24}\frac{\partial^4\psi}{\partial x^4}\right]_{1,j} + O(h^4). \tag{35}$$

As $v_{1,j}$ equals zero, using Eq. (15), we have

TABLE X. Effect of order of accuracy of $\partial T/\partial x$ at $x=0$ and 1 on Nu's.

Ra	Order	$\overline{\mathrm{Nu}}$	Nu_0	$\mathrm{Nu}_{0\max}$ (y)	$\mathrm{Nu}_{0\min}$ (y)
	$O(h^3)$	1.118	1.118	1.505	0.692
10^3				(0.088)	(1.000)
	$O(h^4)$	1.117	1.118	1.505	0.692
				(0.088)	(1.000)
	$O(h^3)$	2.245	2.245	3.527	0.587
10^4				(0.150)	(1.000)
	$O(h^4)$	2.244	2.245	3.528	0.587
				(0.150)	(1.000)
	$O(h^3)$	4.522	4.530	7.710	0.737
10^5				(0.088)	(1.000)
	$O(h^4)$	4.521	4.538	7.730	0.737
				(0.088)	(1.000)
	$O(h^3)$	8.831	8.967	17.789	1.022
10^6				(0.038)	(1.000)
	$O(h^4)$	8.830	9.028	17.980	1.024
				(0.038)	(1.000)
	$O(h^3)$	16.530	17.668	42.369	1.561
10^7				(0.025)	(1.000)
	$O(h^4)$	16.532	17.846	42.175	1.565
				(0.025)	(1.000)

$$0 = \left[-\delta_x^+\psi + \frac{h}{2}\left(-\omega - \frac{\partial^2\psi}{\partial y^2}\right) + \frac{h^2}{6}\left(-\frac{\partial\omega}{\partial x} - \frac{\partial^3\psi}{\partial x\partial y^2}\right) + \frac{h^3}{24}\left(-\frac{\partial^2\omega}{\partial x^2} - \frac{\partial^4\psi}{\partial x^2\partial y^2}\right)\right]_{1,j} + O(h^4).$$

Also in view of the fact that $\partial^2\psi/\partial y^2 = 0$, $\partial^3\psi/\partial x\partial y^2 = \partial^2 v/\partial y^2 = 0$ on the left wall and $\partial^4\psi/\partial x^2\partial y^2 = \partial^3/\partial x\partial y^2(\partial\psi/\partial x) = -\partial^3 v/\partial x\partial y^2$, the above relation becomes

$$0 = \left[-\delta_x^+\psi - \frac{h}{2}\omega - \frac{h^2}{6}\left(\delta_x^+\omega - \frac{h}{2}\frac{\partial^2\omega}{\partial x^2}\right) - \frac{h^3}{24}\left(\frac{\partial^2\omega}{\partial x^2} - \frac{\partial^3 v}{\partial x\partial y^2}\right)\right]_{1,j} + O(h^4).$$

Finally, as $u = v = 0$ on the walls so that Eq. (14) yields $\nabla^2\omega + \mathrm{Ra}\partial T/\partial x = 0$, we get the following fourth-order accurate expression on the left wall:

$$\left[-\delta_x^+\psi - \frac{h}{2}\omega - \frac{h^2}{6}\delta_x^+\omega + \frac{h^3}{24}(-\delta_y^2\omega - \mathrm{Ra}\delta_x^+ T) + \frac{h^3}{24}\delta_x^+\delta_y^2 v\right]_{1,j} = 0. \tag{36}$$

Similarly on the right wall

$$\left[-\delta_x^-\psi + \frac{h}{2}\omega - \frac{h^2}{6}\delta_x^-\omega + \frac{h^3}{24}(\delta_y^2\omega + \mathrm{Ra}\delta_x^- T) - \frac{h^3}{24}\delta_x^-\delta_y^2 v\right]_{mj} = 0. \tag{37}$$

On the bottom wall

$$\left[\delta_y^+\omega + \frac{h}{2}\omega + \frac{h^2}{6}\delta_y^+\omega + \frac{h^3}{24}(\delta_x^2\omega + \mathrm{Ra}\delta_x T) + \frac{h^3}{24}\delta_x^2\delta_y^+ u\right]_{i,1} = 0. \tag{38}$$

On the top wall

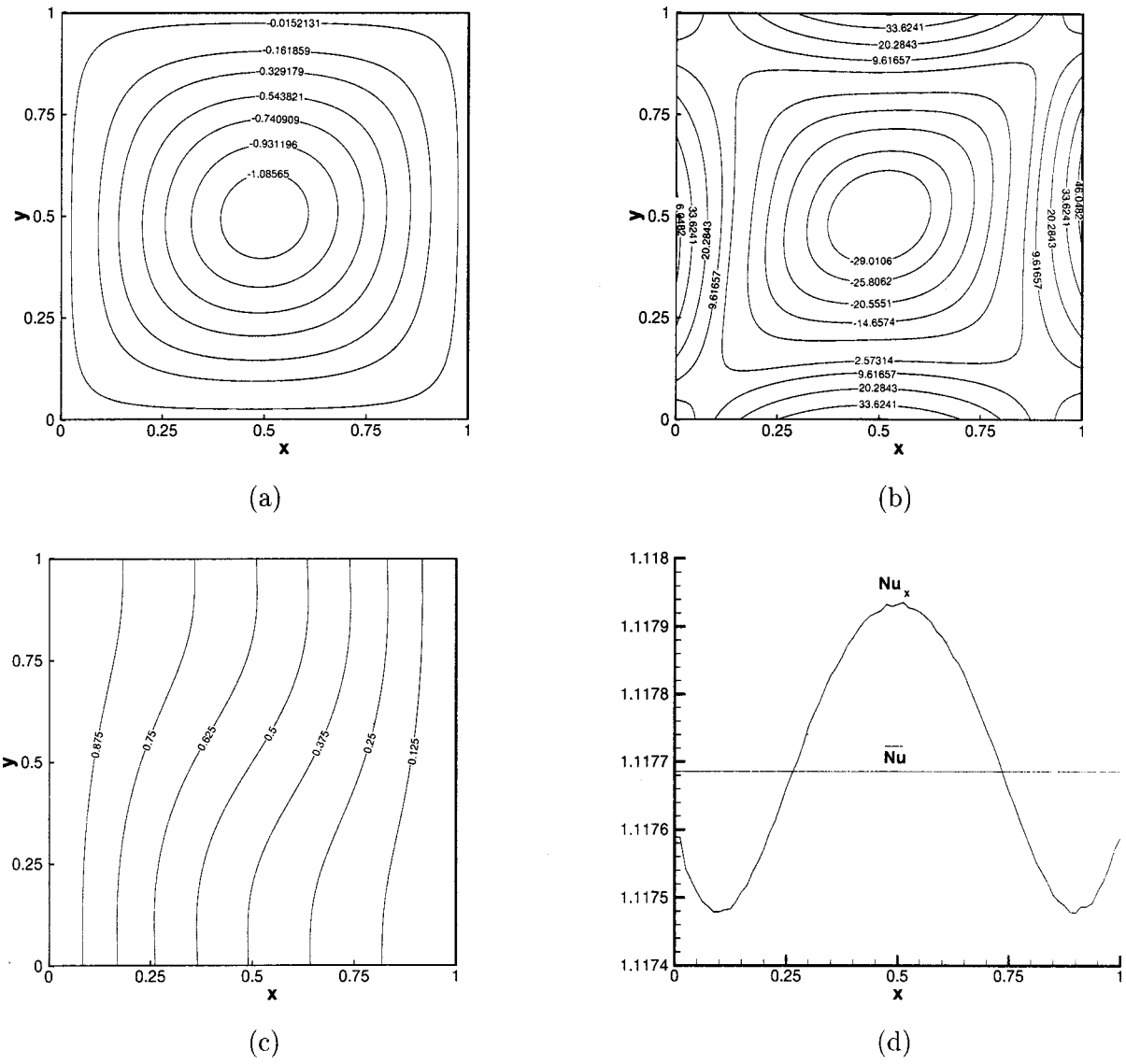

FIG. 2. For $\mathrm{Ra}=10^3$, (a) stream-function contours ($\psi_{\min}=-1.175$), (b) vorticity contours ($\omega_{\min}=-32.02$ and $\omega_{\max}=51.25$), (c) isotherms, (d) the Nusselt number distribution across the cavity.

$$\left[\delta_y^- \psi - \frac{h}{2}\omega + \frac{h^2}{6}\delta_y^-\omega - \frac{h^3}{24}(\delta_x^2\omega + \mathrm{Ra}\,\delta_x T) - \frac{h^3}{24}\delta_x^2\delta_y^- u\right]_{i,m} = 0. \tag{39}$$

Here space indices vary from 1 to m in both x and y directions.

On the insulated top and bottom walls, we now proceed to develop a fourth-order accurate zero-gradient temperature boundary condition. It may be mentioned that as temperature remains constant on the vertical walls, this zero-gradient condition is automatically satisfied at the corners. At a typical node (i,j), we may write

$$0 = \frac{\partial T}{\partial y} = \left[\delta_y T - \frac{h^2}{6}\frac{\partial^3 T}{\partial y^3}\right]_{ij} + O(h^4).$$

As on the boundaries $\nabla^2 T = 0$, the last relation yields

$$0 = \left[\delta_y T + \frac{h^2}{6}\delta_x^2\delta_y T\right]_{ij} + O(h^4).$$

Thus the finite difference approximation of the temperature equation on the insulated boundaries are

$$T_{i+1,j+1} + T_{i-1,j+1} + 4T_{i,j+1} = T_{i+1,j-1} + T_{i-1,j-1} + 4T_{i,j-1}. \tag{40}$$

Again HOC discretization of the energy equation at the walls are given by

$$T_{i+1,j+1} + T_{i-1,j+1} + 4(T_{i+1,j} + T_{i,j+1}T_{i-1,j}) + (T_{i+1,j-1} + T_{i-1,j-1} + 4T_{i,j-1}) - 20T_{ij} = 0. \tag{41}$$

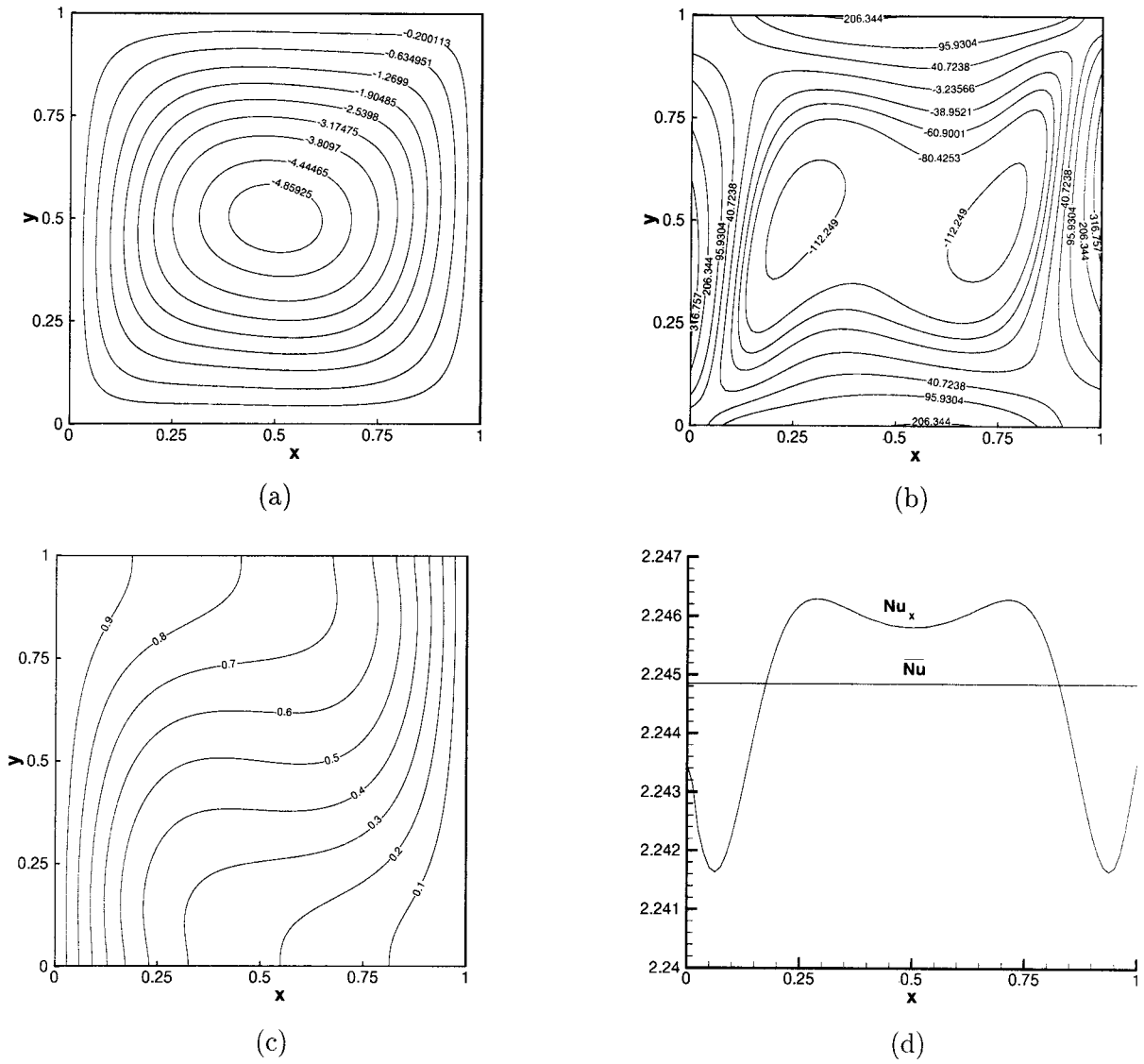

FIG. 3. For $\mathrm{Ra}=10^4$, (a) stream-function contours ($\psi_{\min}=-5.079$), (b) vorticity contours ($\omega_{\min}=-124.90$ and $\omega_{\max}=427.17$), (c) isotherms, (d) the Nusselt number distribution across the cavity.

From Eqs. (40) and (41), it follows that, for the lower boundary

$$T_{i+1,2}+T_{i-1,2}+4T_{i,2}+2(T_{i+1,1}+T_{i-1,1})-10T_{i,1}=0, \tag{42}$$

and for the upper boundary

$$T_{i+1,m-1}+T_{i-1,m-1}+4T_{i,m-1}+2(T_{i+1,m}+T_{i-1,m})-10T_{i,m}=0. \tag{43}$$

This approach used to develop the temperature boundary conditions on the insulated walls can also be extended to similar physical situations for a flow variable ϕ, where, on the boundary, $\partial\phi/\partial n=0$ and $\nabla^2\phi=0$ (n being the direction normal to the boundary). One important situation of this nature could be the pressure Poisson equation with zero pressure gradient boundary conditions, when HOC algorithm is attempted to be extended to the primitive variable formulation of the N-S equations.

IV. NUMERICAL ISSUES

The nonlinearity of the governing equations necessitates an iterative solution procedure. We use a decoupled algorithm where vorticity, stream-function, and temperature are solved in sequence separately, lagging the appropriate terms. The successive iterates for the temperature have been slightly over-relaxed and that for stream-function and vorticity have been under-relaxed. That is to say, if ϕ' is the unrelaxed update of ϕ^n, then ϕ^{n+1} is given by

$$\phi^{n+1}=\lambda\phi'+(1-\lambda)\phi^n,$$

where λ is the relaxation factor and the superscripts n and $n+1$ are iteration indices.

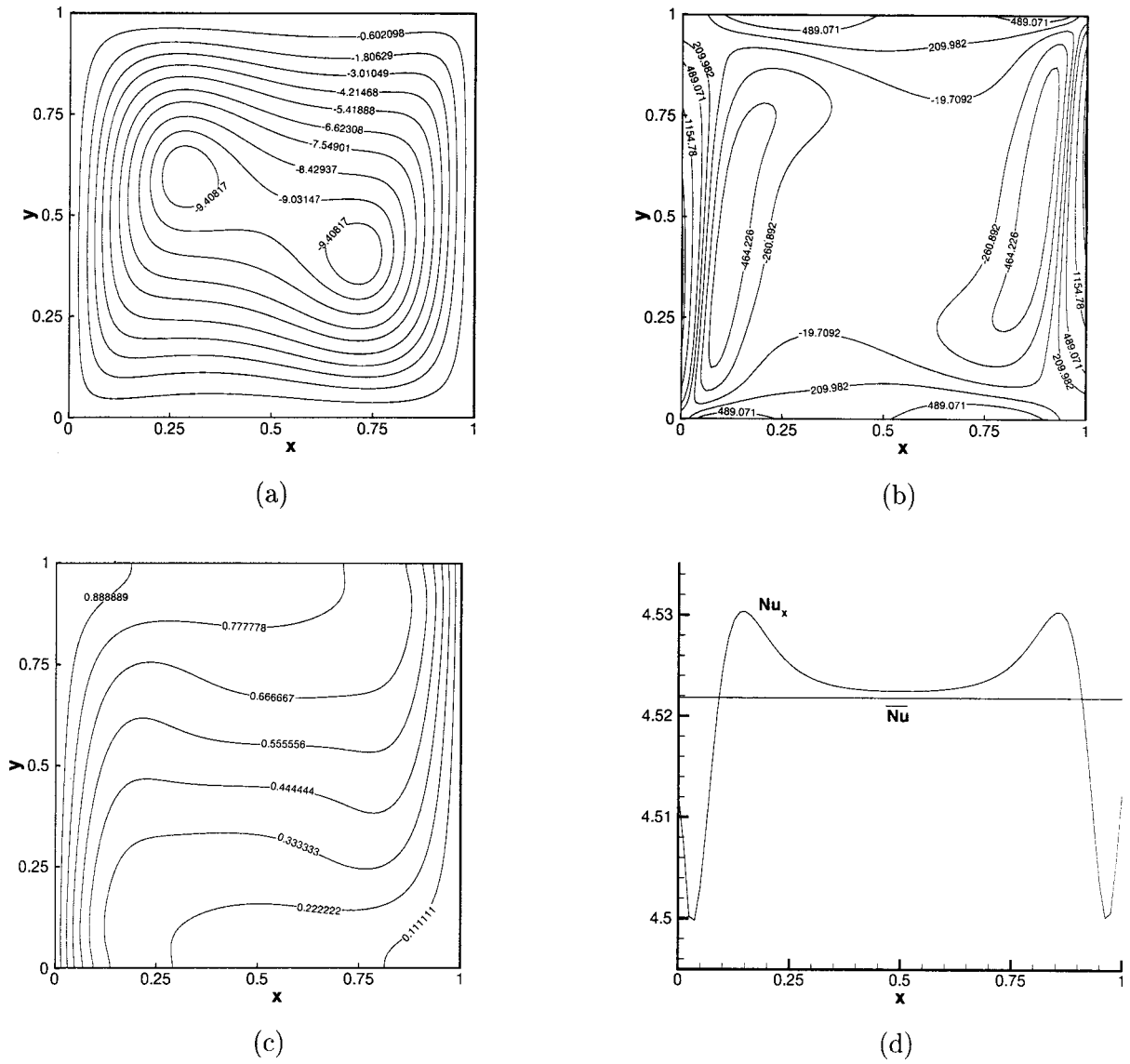

FIG. 4. For $\mathrm{Ra}=10^5$, (a) stream-function contours ($\psi_{\min}=-9.633$), (b) vorticity contours ($\omega_{\min}=-606.95$ and $\omega_{\max}=2622.89$), (c) isotherms, (d) the Nusselt number distribution across the cavity.

Again, the coefficient matrices resulting from the HOC discretization are not diagonally dominant [17] and, therefore, iterative techniques like Gauss-Seidel cannot be applied here. As the coefficient matrix for the stream-function is symmetric and positive definite, the CG [15] algorithm has been used, and those for the vorticity and temperature being nonsymmetric, a hybrid BiCGStab [16] algorithm has been employed.

For computational advantage, the computed solution for a lower Ra can be used as the initial guess for a higher Ra. The vorticity, stream function, and temperature equations are solved in that order. The CG and hybrid BiCGStab iterations used for solving these equations to a certain accuracy are termed as inner iterations. The process of iteratively solving the three equations once may be termed as one outer iteration that is to be repeated until convergence is achieved. It may be noted that the number of inner iterations needed to meet a particular stopping criterion generally reduces with the progress of outer iterations. If the systems associated with ψ, ω, and T equations are represented by $A\mathbf{z}=\mathbf{b}$, the inner iterations are terminated here as soon as the residual $\|A\mathbf{z}-\mathbf{b}\|_2$ falls below 10^{-10}. Convergence is considered to be achieved when the maximum difference between two successive iterates for all of ψ, ω, and T falls below 10^{-10}.

It may be noted that for an $n\times n$ grid, A is an $n^2\times n^2$ matrix and $\mathbf{z}$ and $\mathbf{b}$ are n^2-component vectors. However, the actual storage required for A is much less than $n^2\times n^2$ words, as the algorithm requires the storage of only the nonzero elements of A. The number of nonzero entries of A for ω, ψ, and T equations are $9n^2-20n+24$, $9n^2-32n+32$, and $9n^2-22n+12$, respectively. A condition number analysis based on a power method for eigenvalues, shows that the matrices are well conditioned, the value of the condition number generally being less than 1.3. This is the reason why no need for preconditioning was felt when using the CG and

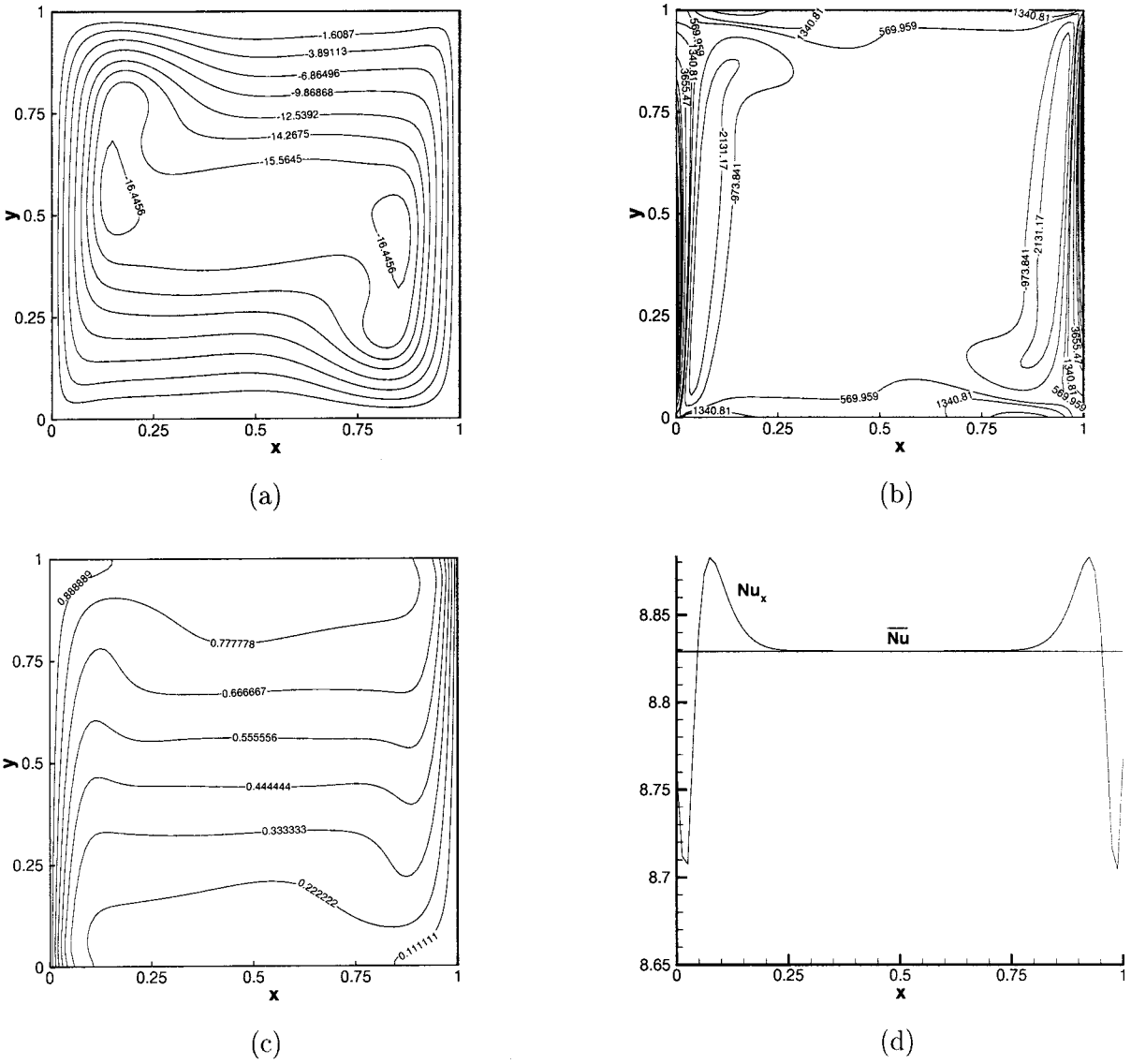

FIG. 5. For $Ra=10^6$, (a) stream-function contours ($\psi_{min}=-16.86$), (b) vorticity contours ($\omega_{min}=-3288.5$ and $\omega_{max}=1528.8$), (c) isotherms, (d) the Nusselt number distribution across the cavity.

hybrid BiCGStab algorithms. All computations in this work were carried out on a HP C 200 machine using a sequential code.

V. RESULTS AND DISCUSSION

In this section, besides discussing other aspects, we also examine the accuracy of the present fully compact higher-order accurate algorithm by comparing its results with already existing results. They are presented here through tables and graphs for Ra's ranging from a moderate 10^3 to a high laminar 10^7. Tables I, II, III, and IV present the results for $Ra=10^3$ to 10^6 for grids of size 21×21, 41×41, and 81×81. Table V shows the results for $Ra=10^7$ on a 81×81 grid. The quantities presented here are the stream function ψ_{mid} at the midpoint of the cavity, the maximum horizontal velocity u_{max} on the vertical midplane together with its location, the maximum vertical velocity v_{max} on the horizontal midplane together with its location, the average Nusselt number $\overline{Nu}$, the average Nusselt number $Nu_{1/2}$ on the vertical midplane of the cavity, the average Nusselt number Nu_0 on the hot wall, the maximum and minimum values $Nu_{0\,max}$ and $Nu_{0\,min}$ of the local Nusselt number on the hot wall together with their locations, and the CPU time in seconds. The grid independence of the results is evident from the first four tables as the variation in results is insignificantly small (Table VI) with grid refinement. Owing to high-order (viz fourth) accuracy of both the scheme and the boundary conditions, high quality solutions are obtained with as coarse a grid as 21×21. This comes out clearly from Tables VII, VIII, and IX, where the computed values of $|\psi_{mid}|$, $\overline{Nu}$, and v_{max} are compared with some well established results and the agreement is found to be excellent. The Nusselt numbers that are presented in Tables I, II, III, IV, and V are calculated using the first-order approximation to $\partial T/\partial x$ at the vertical walls. The same Nusselt numbers esti-

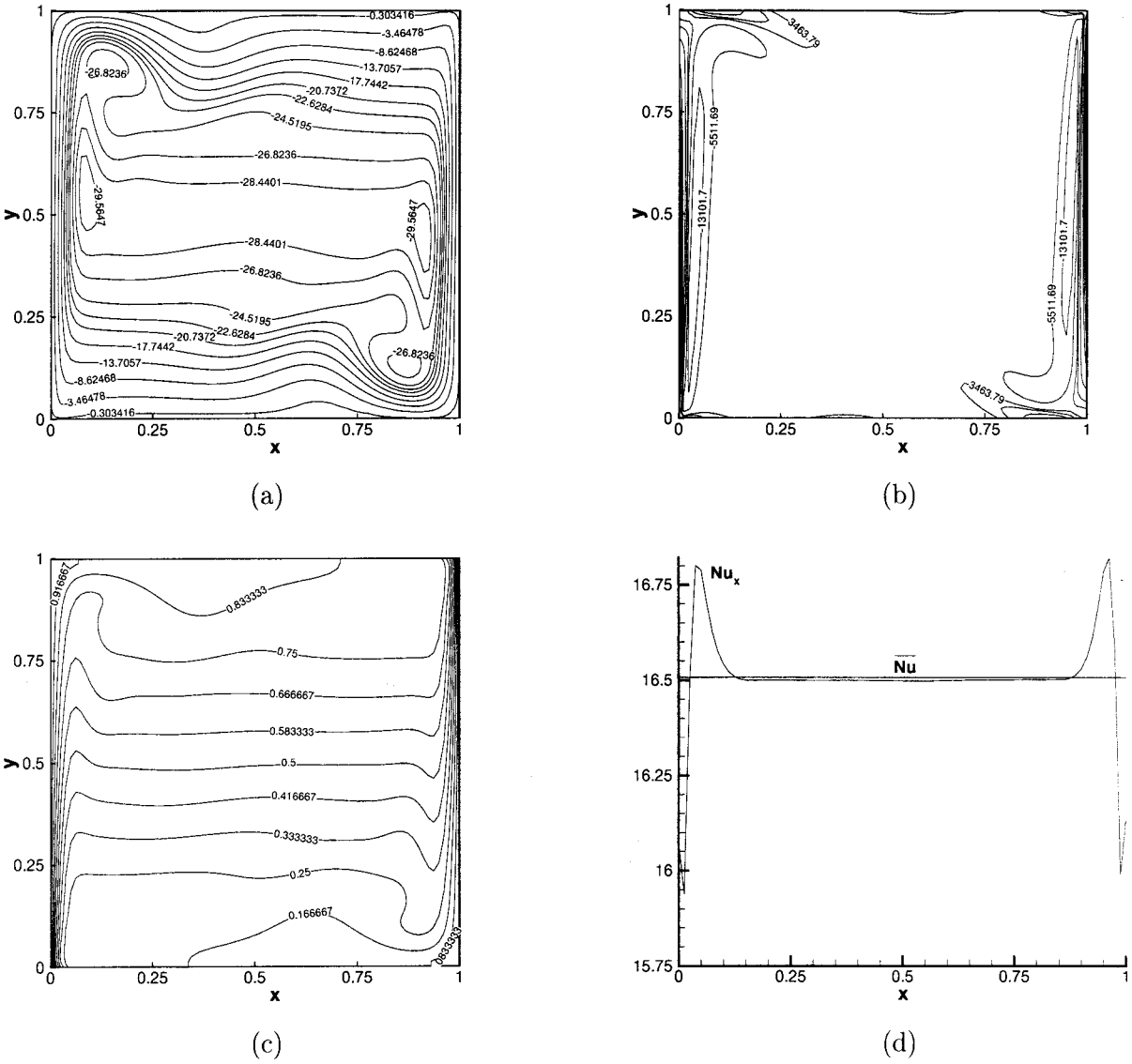

FIG. 6. For $Ra=10^7$, (a) stream-function contours ($\psi_{min}=-30.32$), (b) vorticity contours ($\omega_{min}=-18\,610$ and $\omega_{max}=86\,313.5$), (c) isotherms, (d) the Nusselt number distribution across the cavity.

mated through the use of the third- and fourth-order Jensen formulas [18] are presented in Table X. Comparisons among these Nusselt numbers clearly show that, except for the values of Nu_0 and $Nu_{0\,max}$ calculated with the first-order formula at $Ra=10^7$, all the other estimates are in very close agreement, in particular, the values calculated with third- and fourth-order formulas.

Figure 2 shows the stream-function contours, the vorticity contours, isotherms and the Nusselt number distribution in the cavity for $Ra=10^3$. Figures 3–6 show the same for $Ra=10^4-10^7$, respectively. The contours and distributions bear very close resemblance with similar figures presented by De Vahl Davis [4], Le Quéré [8], Ramaswamy, Jue, and Akin [7], Chenoweth and Paolucci [5], and Hortmann, Peric, and Scheure [6].

De Vahl Davis [4] obtained his results using an FTCS scheme of second-order spatial accuracy in conjunction with Richardson extrapolation; similarly Chenoweth and Paolucci [5] used a second-order accurate method followed by a three point Richardson extrapolation and claimed their results to be sixth-order accurate. It may, however, be noted that these extrapolated solutions are obtained only at those nodes that are shared by different levels of grids. Previously, the need to use extrapolation to obtain higher-order accurate solution using a lower-order accurate scheme was probably necessitated by the absence of well-examined HOC schemes. In contrast, the present work obtains high quality solutions with a fourth-order fully HOC scheme on a single coarse grid. The computations use De Vahl Davis' nondimensionalization to obtain reasonably accurate solutions even for a Rayleigh number as high as 10^7, although Le Quéré [8] remarked that De Vahl Davis' dimensionless form is inappropriate for the Rayleigh number regime beyond 10^6 and used a slightly different scaling.

For the range of Rayleigh numbers considered here, there is generally a centro symmetry of velocity, vorticity, and temperature distribution. This is obvious from the streamline and vorticity contours and the isotherms in parts (a), (b), and

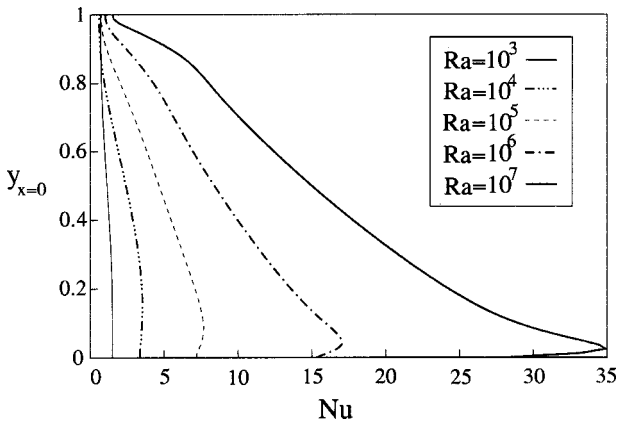

FIG. 7. The variation of Nusselt numbers across the hot wall for different Ra's.

(c) of Figs. 2, 3, 4, 5, and 6. At $Ra=10^7$, recirculation regions are seen to appear at the upper left and lower right corners [Fig. 6(a)]. From part (d) of Figs. 2, 3, 4, 5, and 6, the distribution of Nu_x is seen to be symmetric about the central vertical line. At $Ra=10^3$, there is one peak located at the axis of symmetry and for the other Ra's there exist two peaks symmetrical about the axis moving further and further away from it as Ra increases. Figure 7 shows that the location of the maximum local Nusselt number at the hot wall progressively moves down as Ra increases. Secondary vortices appear at $Ra=10^5$ and persist for higher Ra's. From part (b) of Figs. 2, 3, 4, 5, and 6, on the vertical walls, boundary layer thickness is seen to progressively decrease as Ra increases. These observations tally with those of earlier investigators.

VI. CONCLUSION

This work is concerned with HOC computation of the standard thermally driven square cavity problem with adiabatic horizontal walls and differentially heated vertical walls for values of Ra varying from 10^3 to 10^7. In the previous (probably only) example of HOC computation [13] for this problem, the difficult cases of $Ra=10^6$ and 10^7 have not been studied. Also, the boundary conditions are not compact and the derivative source term that appears in the vorticity equation (viz. $\partial T/\partial x$) has been resolved at least to second-order accuracy. The present work, besides including the results for the high Rayleigh numbers of $Ra=10^6$ and 10^7, employs an algorithm that is uniformly fourth-order accurate and compact in the discretization of the governing equations, treatment of the boundary conditions and source term resolution. This is the reason why the solution procedure may be termed as a fully compact higher-order method with the associated advantages. The no-heat-flux boundary condition at the adiabatic walls has been imposed through a special strategy taking care to maintain compactness at higher accuracy. This technique has the potential of being extended to other similar physical situations. The work also achieves higher-order compact resolution of the source term and its easy assimilation into the solution procedure. This opens up new possibilities of this strategy being extended to situations like pressure gradient term in the primitive variable formulation of the N-S equations. Hence, a complete HOC primitive variable formulation of the N-S equations is now possible that can further be extended to three-dimensions as well. Another fact that we come across in course of the work is that Le Quéré's [8] observation about De Vahl Davis' nondimensionalization [4] being not adequate beyond $Ra=10^6$ may not be correct as computation has been carried out here with the same nondimensionalization with sufficient accuracy. Also, in the course of the estimation of the hot wall Nusselt numbers, De Vahl Davis [4] observed that varying the order of approximation of the finite difference formulas produced significantly different values. But in the present calculations, close agreement among the Nusselt numbers estimated through approximation of $\partial T/\partial x$ at the vertical walls with formulas of three different orders show that the solutions obtained by us are indeed very accurate. Finally, use of CG and hybrid BiCGStab algorithms to solve the symmetric and nonsymmetric algebraic systems at every outer iteration makes the solution procedure robust. The method also has the advantage that the fully HOC method used provides matrices that are well conditioned and hence the complexity of constructing an efficient preconditioner is avoided.

ACKNOWLEDGMENTS

J.C.K. would like to express his thanks to the University Grants Commission, India for supporting his research work.

[1] G. De Vahl Davis and I. P. Jones, Int. J. Numer. Methods Fluids **3**, 227 (1983).
[2] D. C. Dalal, N. Datta, and S. K. Mukherjea, Int. J. Heat Mass Transf. **41**, 547 (1998).
[3] J. O. Wilkes and S. W. Churchill, AIChE J. **12**, 161 (1966).
[4] G. De Vahl Davis, Int. J. Numer. Methods Fluids **3**, 249 (1983).
[5] D. R. Chenoweth and S. Paolucci, J. Fluid Mech. **169**, 173 (1986).
[6] M. Hortmann, M. Peric, and G. Scheure, Int. J. Numer. Methods Fluids **11**, 189 (1990).
[7] B. Ramaswamy, T. C. Jue, and J. E. Akin, AIAA J. **30**, 412 (1992).
[8] P. Le Quéré, Comput. Fluids **1**, 29 (1991).
[9] R. J. A. Janssen and R. A. W. M. Henkes, Numer. Heat Transfer **24**, 191 (1993).
[10] Toshio Tagawa and Hiroyuki Ozoe, Numer. Heat Transfer **30**, 272 (1996).
[11] C. J. Ho and F. H. Lin, Numer. Heat Transfer **31**, 881 (1997).
[12] G. Comini, G. Cortella, and M. Manzan, Numer. Heat Transfer **28**, 1 (1995).
[13] S. C. R. Dennis and J. D. Hudson, J. Comput. Phys. **85**, 390 (1989).
[14] W. F. Spotz and G. F. Carey, Int. J. Numer. Methods Eng. **38**,

3497 (1995).
[15] C. T. Kelly, *Iterative Methods for Linear and Nonlinear Equations* (SIAM Publications, Philadelphia, 1995).
[16] G. L. G. Sleijpen and H. A. Van der Vorst, in *Computational Fluid Dynamics Review*, edited by M. Hafez and K. Oshima (John Wiley and Sons, Chichester, 1995).
[17] W. F. Spotz and G. F. Carey, Texas Institute of Computational and Applied Mechanics Technical Report No. 94-03, 1994 (unpublished).
[18] W. F. Spotz, Int. J. Numer. Methods Fluids **28**, 737 (1998).
[19] T. Saitoh and K. Hirosh, Comput. Mech., Berlin **4**, 417 (1989).
[20] K. S. Ball and D. C. Kuo, J. Heat Transfer **2**, 313 (1994).